

# Loss mechanisms in superconducting thin film microwave resonators

Jan Goetz,<sup>1, 2, a)</sup> Frank Deppe,<sup>1, 2, 3</sup> Max Haeberlein,<sup>1, 2</sup> Friedrich Wulschner,<sup>1, 2</sup> Christoph Zollitsch,<sup>1, 2</sup> Sebastian Meier,<sup>1, 2</sup> Michael Fischer,<sup>1, 2</sup> Alexander Baust,<sup>1, 2, 3</sup> Peter Eder,<sup>1, 2, 3</sup> Edwar Xie,<sup>1, 2, 3</sup> Kirill G. Fedorov,<sup>1, 2</sup> Edwin P. Menzel,<sup>1, 2</sup> Achim Marx,<sup>1</sup> and Rudolf Gross<sup>1, 2, 3, b)</sup>

<sup>1)</sup> Walther-Meissner-Institut, Bayerische Akademie der Wissenschaften, 85748 Garching, Germany

<sup>2)</sup> Physik-Department, Technische Universität München, 85748 Garching, Germany

<sup>3)</sup> Nanosystems Initiative Munich (NIM), Schellingstraße 4, 80799 München, Germany

(Dated: prel. version 21 October 2015)

We present a systematic analysis of the internal losses of superconducting coplanar waveguide microwave resonators based on niobium thin films on silicon substrates. At millikelvin temperatures and low power, we find that the characteristic saturation power of two-level state (TLS) losses shows a pronounced temperature dependence. Furthermore, TLS losses can also be introduced by Nb/Al interfaces in the center conductor, when the interfaces are not positioned at current nodes of the resonator. In addition, we confirm that TLS losses can be reduced by proper surface treatment. For resonators including Al, quasiparticle losses become relevant above 200 mK. Finally, we investigate how losses generated by eddy currents in the conductive material on the backside of the substrate can be minimized by using thick enough substrates or metals with high conductivity on the substrate backside.

## I. INTRODUCTION

Superconducting microwave transmission line resonators are widely used in circuit quantum electrodynamics (QED) to study light-matter interaction,<sup>1, 2</sup> as quantum bus<sup>3, 4</sup> or photon storage devices.<sup>5</sup> For many of those applications, the coherence time limited by internal loss channels of the resonator should be as long as possible. In the single photon limit, two-level states (TLSs) located at the metal/substrate, metal/air, and substrate/air interfaces are considered to be the main contributors to microwave losses.<sup>6, 7</sup> In order to reduce these losses, much effort has been put into material development focusing on different metallization compounds<sup>8, 9</sup> or substrate materials.<sup>10, 11</sup> Also, quasiparticle generation in the superconducting material from stray infrared light<sup>12</sup> or thermal activation<sup>13</sup> generates losses in these resonators. In addition to material choice and screening quality, the sample design itself can have a large influence on the internal quality factor of the resonator.<sup>14, 15</sup> This influence can arise from impedance mismatches at the coupling ports resulting in Fano resonances,<sup>16, 17</sup> from parasitic modes in the substrate,<sup>18</sup> or from additional resistive loss channels.<sup>19</sup> Furthermore, Josephson junctions which are galvanically coupled to the resonator can contribute to microwave losses.<sup>20</sup> For efficiently shielded and well designed setups based on optimized materials, internal quality factors above one million have been reached.<sup>17</sup>

In this work, we investigate three independent parameters affecting the internal losses of superconducting thin film resonators. We first evaluate TLS losses in Nb coplanar waveguide (CPW) resonators and evaluate the in-

fluence of a SiO<sub>2</sub> layer on top of the Si substrate. In addition, we observe a temperature dependence in the characteristic saturation power of the TLSs in agreement with TLS theory.<sup>21, 22</sup> Second, we analyze the influence of Nb/Al interfaces in the center conductor of a CPW resonator. Such interfaces are unavoidable in the galvanic coupling of circuits made from Al-based Josephson junctions to a Nb resonator. Third, we analyze losses introduced by eddy currents in the conductive material used to attach our samples to the sample box. To this end, we study the influence of the substrate thickness and find that the impact of the eddy current losses increases with decreasing substrate thickness.

## II. EXPERIMENTAL TECHNIQUES

We first introduce our measurement setup and the most relevant fabrication steps. We systematically study the internal losses of one microstrip (MS) and eight CPW resonators with parameters as summarized in Table I. For electrical characterization, all samples discussed here are fixed with silver glue inside a gold-plated copper box as shown in Fig. 1(a) and cooled down to the temperature of the cold-stage of a dilution refrigerator which can be stabilized between 50 mK and 600 mK with a precision of  $\pm 0.1$  mK. Our low temperature setup has a radiation shield at 700 mK, a cryoperm shield at 4.2 K, and  $\mu$ -metal shielding at room temperature. The input lines are heavily attenuated at different temperature levels in order to achieve populations of less than one photon on average inside the resonator. In the output lines we use cryogenic circulators mounted on the sample stage and on the 700 mK plate for this purpose. We amplify the signal using a high electron mobility transistor amplifier at 4.2 K and one additional room temperature amplifier. Measurements are performed with a vector network analyzer (VNA).

<sup>a)</sup>jan.goetz@wmi.badw.de

<sup>b)</sup>rudolf.gross@wmi.badw.de

TABLE I. Overview of the samples analyzed in this work. The values of  $\delta_{\text{TLS}}^0$ ,  $\delta_c$ ,  $\beta$  and  $P_c$  are obtained by fitting Eq. (1) to a power sweep of each individual sample as shown in Fig. 4. We also list confidence intervals generated by the fits. We obtain  $\alpha$  by fitting Eq. (3) to the values of  $P_c(T)$ . \* Sample IX has a superconducting groundplane on the backside of the substrate.

ID	Substrate, thickness	Cleaning	Options	$\delta_{\text{TLS}}^0/10^{-5}$	$\delta_c/10^{-5}$	$\beta$	$P_c$ (dBm)	$\alpha$
I	○ Si/SiO <sub>2</sub> , 250 μm	—	—	0.71 ± 0.07	2.08 ± 0.13	0.76 ± 0.06	-97 ± 6	2.3
II	● Si/SiO <sub>2</sub> , 525 μm	—	—	0.89 ± 0.17	1.04 ± 0.29	1.25 ± 0.20	-93 ± 4	2.8
III	▲ Si/SiO <sub>2</sub> , 525 μm	—	EBL	0.34 ± 0.07	0.33 ± 0.09	1.06 ± 0.04	-99 ± 1	—
IV	◆ Si, 250 μm	HF-dip	—	0.09 ± 0.04	3.03 ± 0.51	0.92 ± 0.18	-83 ± 5	2.0
V	◀ Sapphire, 200 μm	Ion gun	—	0.16 ± 0.06	3.84 ± 0.31	1.26 ± 0.56	-83 ± 8	2.8
VI	▼ Si/SiO <sub>2</sub> , 525 μm	—	gridded ground plane	1.19 ± 0.13	0.99 ± 0.11	1.2 ± 0.16	-109 ± 1	—
VII	◆ Si/SiO <sub>2</sub> , 250 μm	Nb/Al: Ion gun	Al bridge	0.86 ± 0.18	1.75 ± 0.23	1.28 ± 0.20	-94 ± 4	2.6
VIII	▶ Si/SiO <sub>2</sub> , 250 μm	—	Al bridge	19.02 ± 0.67	2.78 ± 0.25	1.04 ± 0.02	-124 ± 3	2.4
VIII	▶ Si/SiO <sub>2</sub> , 250 μm	Nb/Al: Ion gun	second harm.	0.69 ± 0.81	1.69 ± 0.36	0.88 ± 0.13	-98 ± 4	2.7
IX	■ Si/SiO <sub>2</sub> , 250 μm	—	*	25.12 ± 1.11	1.14 ± 0.21	2.96 ± 0.04	-110 ± 1	—

We investigate half-wavelength resonators which have resonance frequencies of approximately 4 GHz. Our samples are fabricated either on a SiO<sub>2</sub>-covered silicon, HF treated Si/SiO<sub>2</sub>, or a sapphire substrate.<sup>23</sup> The SiO<sub>2</sub> is thermally grown and the silicon is undoped with a specific resistance larger than 1 kΩ cm. Onto these substrates we sputter-deposit a 100 nm thick Nb film. The resonators are patterned into these films using optical lithography (OL) or electron beam lithography (EBL) and reactive ion etching. The CPW resonators are comprised of a 20 μm wide center conductor separated from the ground plane by a  $w = 12$  μm wide gap on either side. The MS resonator has a conductor width of 200 μm and a 100 nm thick Nb layer on the backside of the substrate serving as ground. We compare samples with different substrate thicknesses and surface treatments to our standard process for Nb on a 250 μm thick silicon substrate covered with 50 nm SiO<sub>2</sub> on both sides (cf. sample I in Tab. I). For sample II and sample III, we use a substrate which is 525 μm thick and we compare OL and EBL. As a surface treatment, we remove the SiO<sub>2</sub> layer on top of

the silicon substrate for sample IV using hydrofluoric acid (HF). To this end, we wet-etch for three minutes with a ratio HF:H<sub>2</sub>O = 1:10. Afterwards, we rinse the sample with deionized water before placing it in the sputtering chamber within five minutes after the wet etch. Sample V is fabricated on a 200 μm thick sapphire substrate, which is in-situ cleaned by Ar ion beam etching before Nb sputter deposition. Sample VI has a gridded ground-plane as shown in Fig. 1 (b). The square holes have a width of 8 μm and are separated by 12 μm. Sample VII and sample VIII are used to investigate the influence of Nb/Al interfaces in the center conductor of the resonator. For this purpose, we replace a 150 μm long piece of the Nb center conductor by an Al strip of identical width and thickness as shown in Fig. 1 (c). The Al strip shares an 100 μm long overlap with the Nb center conductor and is evaporated in an extra fabrication step. For sample VII, we additionally clean the Nb surface by means of in-situ Ar-ion milling before the Al evaporation to remove oxides and resist residues from the Nb surface.

### III. METHODS

In this section we discuss the different contributions to microwave losses which we take into account in our analysis. An overview of these contributions is given in Fig. 2. In order to compare the internal losses of devices with different resonance frequencies  $\omega_r/2\pi$ , we calculate the internal quality factor as  $Q_i = 1/(Q_\ell^{-1} - Q_x^{-1})$ . Here,  $Q_\ell$  and  $Q_x$  are the loaded and the external quality factor, respectively. From VNA spectroscopy measurements we obtain the loaded quality factor  $Q_\ell = \omega_r/\Delta\omega$ , where  $\Delta\omega$  is the full width at half maximum of the Lorentzian peak. We use a combination of microwave simulations and reference measurements to obtain  $Q_x \simeq 3 \times 10^5$  for the CPW samples. This external quality applies for all resonators as they share the same layout for the coupling capacitor shown in Fig. 1 (d).

For our analysis, we calculate the losses  $\delta_i = 1/Q_i$ , where  $\tan \delta_i$  is the well-known loss tangent. We split the

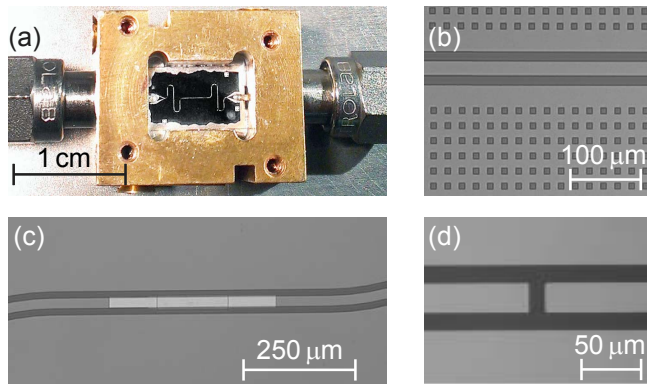


FIG. 1. (a) Photograph of a resonator sample fixed with silver glue in a gold-plated copper box. (b) Micrograph of sample VII at the position where the Nb center conductor is replaced by an Al strip. (c) Micrograph of a typical coupling capacitor used for the CPW samples.

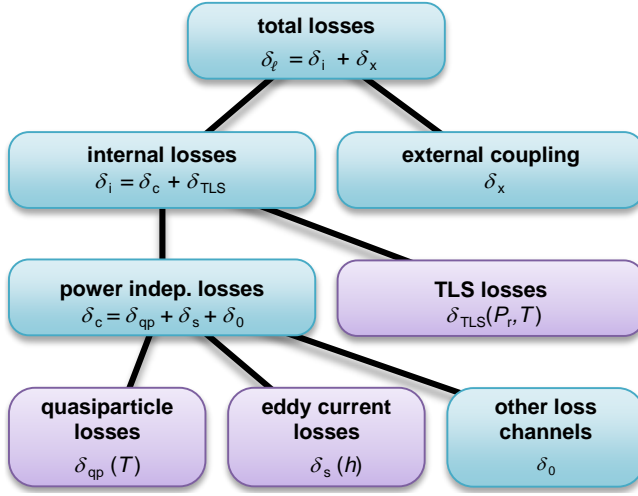


FIG. 2. Microwave loss contributions. Due to our knowledge of the contribution  $\delta_x$  from the coupling capacitors, our measurements of the total losses allow for a detailed discussion of TLS, quasiparticle, and eddy current losses (violet boxes). The quasiparticle losses are obtained from the Nb/Al samples and the eddy current losses via their dependence on the substrate thickness  $h$ .

internal losses into a power independent term  $\delta_c$  and a power and temperature dependent TLS contribution  $\delta_{\text{TLS}}(P_r, T)$ . Hence, the internal losses read are described as

$$\delta_i(P_r, T) = \delta_{\text{TLS}}(P_r, T) + \delta_c. \quad (1)$$

Here,  $P_r = P Q_\ell^2 / n \pi Q_x$  is the power circulating inside the resonator<sup>8</sup> for the  $n^{\text{th}}$  mode and  $P$  is the power resonantly applied to the input of the resonator. In Eq. (1)  $\delta_{\text{TLS}}(P_r, T)$  describes the losses due to the coupling of an ensemble of microscopic TLSs to the electromagnetic field of the resonator. These TLSs are located inside the dielectric and at the dielectric/metal interfaces in the vicinity of the resonator. For such a system, the TLS contribution reads<sup>8,24</sup>

$$\delta_{\text{TLS}}(P_r, T) = \delta_{\text{TLS}}^0 \frac{\tanh(\hbar\omega_r/2k_B T)}{\sqrt{1 + (P_r/P_c)^{\beta/2}}}. \quad (2)$$

In this expression, the exponent  $\beta$  is known to be design-dependent,<sup>25</sup>  $P_c$  is a characteristic power depending on the TLS properties,<sup>11,26</sup> and  $k_B$  is the Boltzmann constant. In the low temperature and low power limit, the internal losses approach  $\delta_{\text{TLS}}^0$  which is mainly limited by the unsaturated TLSs. The characteristic power  $P_c$  is proportional to  $(\tau_1 \tau_\phi)^{-1}$ , where  $\tau_1$  and  $\tau_\phi$  represent the relaxation time of the TLSs and the broadening of the levels due to their mutual interaction, respectively.<sup>26</sup> In the spin-boson model, the temperature dependence of  $\tau_1^{-1}$  follows a  $\coth(\hbar\omega/2k_B T)$  dependence<sup>21,27</sup> which is proportional to  $T$  for  $k_B T \gg \hbar\omega$ . Due to phonon mediated interaction between the TLSs one expects  $\tau_\phi^{-1} \propto \tau_{\text{ac}}^{-1} T + \tau_{\text{op}}^{-1} / [\exp(\hbar\omega/k_B T) - 1]$ , where

$\tau_{\text{ac}}^{-1}$  and  $\tau_{\text{op}}^{-1}$  describe the TLS coupling rate to acoustic and optical phonons, respectively.<sup>28,29</sup> For low temperatures,  $k_B T \ll \hbar\omega$ , the interaction is predominantly mediated by the term accounting for acoustic phonons  $\tau_{\text{ac}}^{-1} T$ . However, in the regime  $\hbar\omega \simeq k_B T$  which is relevant for our experiments, a power law  $\propto T^\alpha$  has been found for both,  $\tau_1^{-1}$  and  $\tau_\phi^{-1}$ .<sup>22,24,26-31</sup> Therefore, the temperature dependence of the characteristic power can be approximated as<sup>26</sup>

$$P_c(T) = \frac{3\hbar^2 \varepsilon}{2d^2 \tau_1(T=0) \tau_{\text{ac}}} \coth\left(\frac{\hbar\omega_r}{2k_B T}\right) T^\alpha, \quad (3)$$

where  $\varepsilon = \varepsilon_0 \varepsilon_r$  is the absolute permittivity of the dielectric and  $d$  is the effective dipole moment of the TLSs. For resonators made from a single metal layer, these TLSs couple mainly to the electric field  $\mathbf{E}_r$  generated by the CPW structure. This situation changes for resonators including metal/metal interfaces, e.g. Nb/Al interfaces, especially if these interfaces include an oxide layer of finite thickness  $h_{\text{ox}}$ . In this case, the interface forms a Josephson junction and the TLSs also couple to the electric field  $|\mathbf{E}_{\text{Nb/Al}}| = V_J/h_{\text{ox}}$  inside this junction.<sup>32</sup> Here,  $V_J = L_J \partial I / \partial t$  is the voltage drop across the junction induced by the resonator current  $I = I_{\omega_r} \cos(\omega_r t)$ . The Josephson inductance is given by  $L_J = \hbar/2eI_c \cos \varphi$ , where  $e$  is the electron charge,  $I_c$  the junction critical current and  $\varphi$  the phase drop across the junction. Hence, the root mean square electric field across the junction reads as

$$E_{\text{Nb/Al}}^{\text{rms}} = \frac{\hbar\omega_r}{2e h_{\text{ox}} \cos \varphi} \frac{I_{\omega_r}}{\sqrt{2} I_c}. \quad (4)$$

Equation (4) shows that a finite resonator current amplitude  $I_{\omega_r}$  leads to a finite electric field across the junction which couples to possible TLSs. Therefore, we can apply Eq. (2) to describe the losses generated by TLSs inside a Josephson junction which is formed by an oxidized metal/metal interface incorporated into the center conductor of a CPW resonator.

In the following, we focus on the high power regime where the internal losses are limited by

$$\delta_c(T, h) = \delta_{\text{qp}}(T) + \delta_s(h) + \delta_0. \quad (5)$$

Here,  $\delta_{\text{qp}}(T)$  are thermally induced quasiparticle losses and  $\delta_s(h)$  are eddy current losses on the backside of the substrate. The term  $\delta_0$  comprises all other loss processes such as radiation,<sup>33</sup> the finite surface resistance of superconductors,<sup>34</sup> and nonthermal quasiparticles generated by stray infrared light.<sup>12,13</sup> Whereas dielectric losses dominate at very low temperatures, the losses related to the superconducting material typically become dominant when the sample temperature exceeds approximately 10 % of the critical temperature  $T_c$  of the superconductor.<sup>11</sup> In the temperature range of our experiments, we expect a considerable quasiparticle contribution only for samples containing Al. Assuming that the superconducting material is in the dirty or local limit,

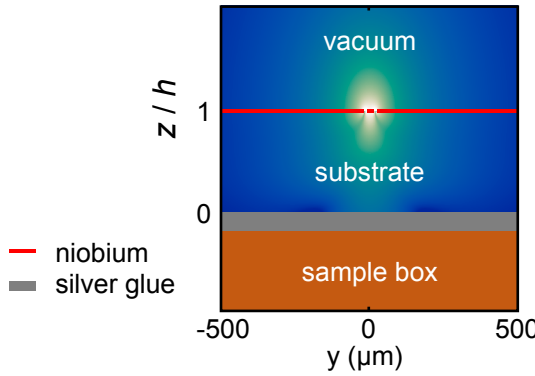


FIG. 3. Energy density (color coded) associated with the resonator magnetic field  $\mathbf{H}(y, z)$  along a  $yz$ -cut through a CPW sample. Depicted in red is the Nb resonator at  $z/h = 1$  with its center conductor at  $y = 0 \mu\text{m}$ . Underneath the sample we use silver glue to attach the substrate to the sample box.

the quasiparticle contribution can be described with the Mattis-Bardeen theory,<sup>13,35</sup>

$$\delta_{\text{qp}}(T) = \frac{2\gamma}{\pi} \frac{e^{-\zeta} \sinh(\xi) K_0(\xi)}{1 - e^{-\zeta} \left( \sqrt{2\pi/\zeta} - 2e^{-\xi} I_0(\xi) \right)}. \quad (6)$$

Here,  $\gamma$  is the ratio of kinetic inductance to total inductance of the conductor,  $\zeta = \Delta_0/k_B T$  with the superconducting energy gap  $\Delta_0$ ,  $\xi = \hbar\omega_r/2k_B T$ , and  $I_0, K_0$  are the modified Bessel function of the first and second kind, respectively.

Eddy current losses  $\delta_s(h)$  in Eq. (5) mainly arise from the finite conductivity of the material used to fix our samples in the sample box. The thickness dependence results from a residual magnetic field  $\mathbf{H}_0 \equiv \mathbf{H}(z=0)$  on the backside of the substrate. Therefore, we also find a finite field  $\mathbf{H}_s$  in the volume of the silver glue used to fix our samples in the sample box (see Fig. 3). Inside the silver glue volume, the field decays exponentially in  $z$ -direction for microwave frequencies within the skin depth  $\lambda$ , thus  $\mathbf{H}_s = \mathbf{H}_0 \exp(-|z|/\lambda)$ . The dissipated power due to eddy currents reads<sup>36</sup>  $P_s = (1/2\sigma_{\omega_r}) \int (\nabla \times \mathbf{H}_s)^2 dV$ , where  $\sigma_{\omega_r}$  is the electrical conductivity at the resonator frequency and  $V$  is the volume of the conductive material on the backside of the substrate. To evaluate the thickness dependence, we calculate the field components of the magnetic field  $\mathbf{H}(x, y, z)$  in the substrate following Ref. 37. We modify this model by appropriate boundary conditions for the conductor-backed substrate demanding the  $z$ -component of  $\mathbf{H}_0$  to vanish. The  $x$ -component of  $\mathbf{H}_0$ , which points in the direction along the transmission line, can also be neglected in comparison with the  $y$ -component. Using these assumptions, the field on the backside of the substrate can be written as  $\mathbf{H}_0(x, y) \approx \hat{e}_y |\mathbf{H}_0(x, y)|$ . Assuming a sinusoidal current distribution along the transmission line, we find  $|\mathbf{H}_0(x, y)| = H_0 k(y, h) \sin(n\pi x/L)$ , where  $L$  is the resonator length and  $k(y, h)$  is the field distribution at  $z = 0$  along the  $y$ -direction. The maximum field

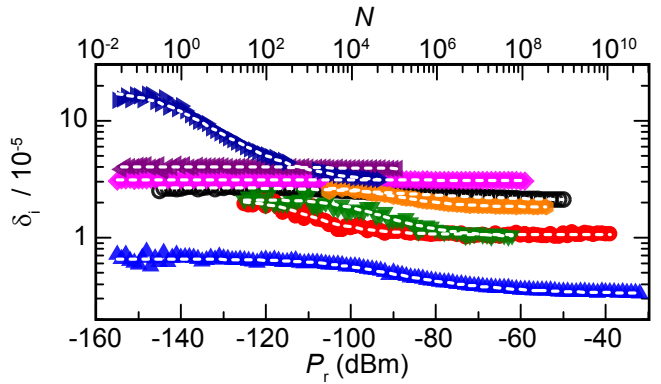


FIG. 4. Internal losses for samples I–VIII plotted versus the microwave power circulating inside the resonator at 50 mK. Symbols are explained in Tab. I. The average photon number on the top axis is calculated as  $N = 2\pi P_r / \hbar\omega_r^2$ . Dashed lines are fits of Eq. (1) to the data.

strength is given as  $H_0 = \sqrt{(1 + \varepsilon_r) P_r Z_0 / 2} (Z_{\text{vac}} w)^{-1}$ . Here,  $Z_0 = 50 \Omega$  and  $Z_{\text{vac}} \simeq 377 \Omega$  are line and vacuum impedance, respectively, and  $\varepsilon_r = 11.9$  is the relative dielectric constant of the Si substrate. Finally, we calculate the dissipated power

$$P_s(h) = \int \frac{dV}{2\sigma_{\omega_r}} \left( \nabla \times \hat{e}_y \frac{H_0 k(y, h) \sin(n\pi x/L)}{\exp(|z|/\lambda)} \right)^2 \approx \sqrt{\frac{\omega_r \mu}{2\sigma_{\omega_r}} \frac{(1 + \varepsilon_r) P_r Z_0 L}{32(Z_{\text{vac}} w)^2}} K(h)^2. \quad (7)$$

In the above expression,  $\int dV = \int_0^L dx \int_{-\infty}^{\infty} dy \int_0^{-\infty} dz$ ,  $\mu \simeq \mu_0$  is the absolute permeability of the conductive material,<sup>38</sup>  $K(h)^2 = \int_{-\infty}^{\infty} k(y, h)^2 dy$  and we use  $\lambda = \sqrt{2/\omega_r \mu \sigma_{\omega_r}}$ .<sup>39</sup> The thickness dependent losses  $\delta_s(h)$  are defined as  $P_s/P_r$ , the ratio of the power dissipated in the system to stored power. Hence,

$$\delta_s(h) = \sqrt{\omega_r \mu / 2\sigma_{\omega_r}} (1 + \varepsilon_r) Z_0 K(h)^2 L / 32(Z_{\text{vac}} w)^2, \quad (8)$$

which is independent of the power circulating inside the resonator.

## IV. RESULTS

In the following, we present the experimental results starting with a comparison of TLS related losses. Next, we show how losses are affected by Nb/Al interfaces which are necessary for the galvanic coupling of Al-based Josephson circuits to the Nb center conductor of the CPW. Finally, we analyze the influence of a finite substrate thickness on internal losses.

### A. TLS losses in Nb resonators

In this subsection, we discuss the TLS losses for samples I–VI (pure Nb resonators). Fitting Eq. (1) to the

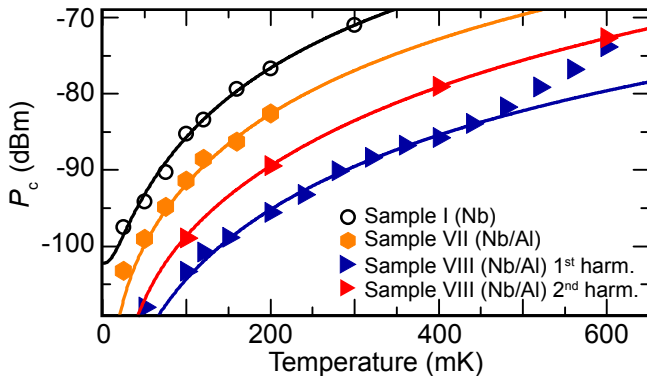


FIG. 5. Characteristic power  $P_c$  plotted versus temperature for different samples. Solid lines are fits of Eq. (3) to the data. For the first harmonic mode of sample VIII we observe a strong increase for temperatures above 440 mK. For this dataset we fit only to datapoints below 440 mK. For better visibility there is a constant offset of  $-4$  dBm and  $16$  dBm for the data of sample VII and sample VIII 1<sup>st</sup> harmonic, respectively.

power dependence of  $\delta_i$ , we extract  $\delta_{\text{TLS}}^0$ ,  $\beta$  and  $P_c$  (see Fig. 4). The results are summarized in Table I. For each individual sample, we observe an increase in  $P_c$  for increasing temperature due to the temperature dependent lifetime of the TLSs as shown in Fig. 5. From a fit based on Eq. (3), we find  $\alpha \simeq 2.5 \pm 0.3$  (average over samples I–VIII). This value deviates from  $\alpha = 1$  expected from the spin-boson model,<sup>21,27</sup> but is comparable to values reported for TLSs in glasses<sup>22,26</sup> and phase qubits.<sup>30,31</sup> The deviation can be attributed to the fact that our experiments are not in the low temperature limit, but rather in the intermediate regime  $\hbar\omega \simeq k_B T$ .

Next, we discuss the low temperature and low power losses  $\delta_{\text{TLS}}^0$ . For sample I, which serves as a reference sample, we find a TLS contribution  $\delta_{\text{TLS}}^0 \simeq 7.1 \times 10^{-6}$ . We now study the influence of TLSs near the surface using sample IV, where we have cleaned the surface with an HF-dip before metallization. For this sample, we measure  $\delta_{\text{TLS}}^0 \simeq 9 \times 10^{-7}$ , which is one order of magnitude lower than for sample I. Hence, we conclude that most of the TLS losses are introduced by the bulk SiO<sub>2</sub> layer, the SiO<sub>2</sub>/metal, and SiO<sub>2</sub>/air surfaces. In contrast, losses at the metal/air interface are significantly smaller ( $\leq 9 \times 10^{-7}$ ). For sample VI (gridded groundplane) the TLS losses are comparable to those of a resonator with continuous groundplane.

## B. Losses due to TLSs at Nb/Al interfaces

We use sample VIII, where an Al strip is placed at the current antinode of the fundamental mode, to study the influence of Nb/Al interfaces introduced into the center conductor of CPW resonators. These interfaces are known to introduce losses in galvanically coupled Joseph-

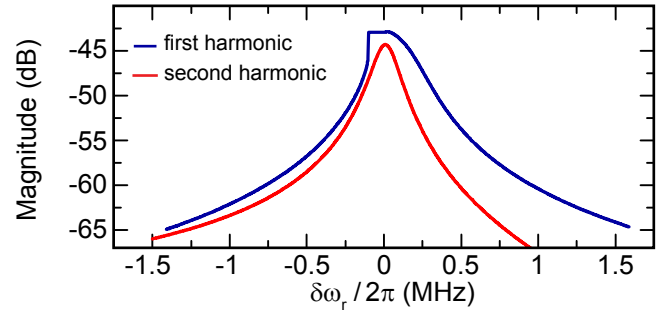


FIG. 6. Transmission magnitude plotted versus  $\delta\omega_r = \omega - \omega_r$  for the first and second harmonic mode of sample VIII at  $P_r \simeq -45$  dBm. For the first harmonic mode, the resonance shows a nonlinear behavior due to the presence of the Nb/Al interface forming a Josephson junction. The second harmonic mode does not couple to the junction and therefore keeps its Lorentzian peak form.

son junction based circuits.<sup>20,40</sup> However, the TLS effect on the internal quality factor of superconducting resonators has not yet been quantified. The transmission of the first harmonic mode of the resonator without ion gun treatment shows a deviation from the Lorentzian lineshape for large probe power (see Fig. 6). As this behavior is typical for resonators including Josephson junctions,<sup>20,41</sup> we treat the Nb/Al interfaces as large-area Josephson junctions. As expected, the second harmonic mode which has a current node at the interface position shows a Lorentzian behavior. Due to the presence of the interfaces, we also observe a non-equidistant mode spacing, which is again typical for resonators including Josephson junctions.<sup>2</sup> Specifically, we find  $\omega_{r,2}/\omega_{r,1} \simeq 1.93$ , where  $\omega_{r,n}$  is the resonance frequency of the  $n^{\text{th}}$  mode. In contrast, all samples without Nb/Al interface (samples I–VI) show an equidistant mode spacing,  $\omega_{r,n}/\omega_{r,1} = n$ .

The presence of the oxidized interfaces results in large TLS losses. For the first harmonic mode of sample VIII, we observe an increase of more than one order of magnitude in  $\delta_{\text{TLS}}^0$  compared to sample I (pure Nb) or sample VII (cleaned Nb/Al interface). Hence, we draw two important conclusions. First, without cleaning step, the Nb oxides present at the interfaces are strong TLS sources. Second, these TLSs can cause significant losses. This behavior is not immediately obvious, because the Nb/Al interfaces are placed at a voltage node of the first harmonic mode. Consequently, the TLSs associated with the Nb oxides at these interfaces are not expected to couple to the resonator electric field. Nevertheless, due to the electric field  $\mathbf{E}_{\text{Nb/Al}}$  between the Nb and the Al layer in the overlap area, we observe a pronounced power and temperature dependence of  $\delta_i$  (see Fig. 7). Actually, according to Eq. (4),  $E_{\text{Nb/Al}}^{\text{rms}}$  is proportional to the resonator current and therefore maximum if the Nb/Al interface is placed at the current antinode (voltage node) of the resonator field.

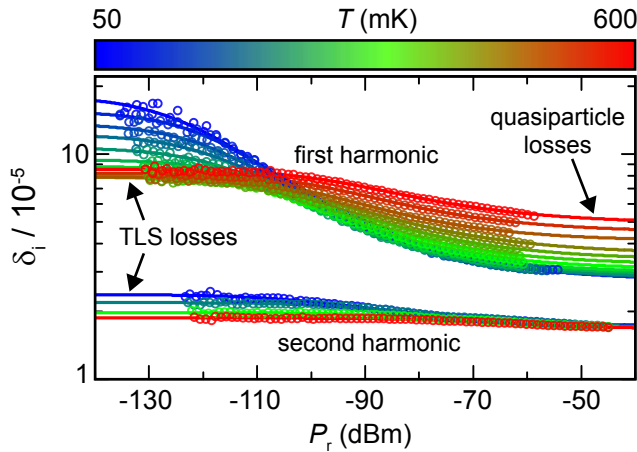


FIG. 7. Internal losses plotted versus the circulating microwave power for the first two harmonic modes of sample VIII (no Ar ion cleaning) at temperatures between 50 mK and 600 mK. Solid lines are fits of Eq. (1) to the data. Arrows indicate the regions relevant for the analysis of TLS and quasiparticle losses.

In the following, we discuss why the TLSs in the interfaces are not yet saturated by  $E_{\text{Nb}/\text{Al}}^{\text{rms}}$  for a probe power corresponding to the vacuum current  $I_{\omega_{r,1}} = \sqrt{\hbar\omega_r^2/2\pi^2Z_0} \simeq 21 \text{ nA}$ . With a junction area of approximately  $2000 \mu\text{m}^2$  and assuming a very low critical current density of  $J_c \simeq 10 \text{ A cm}^{-2}$ ,<sup>42</sup> (the Nb was exposed to air for two days) we estimate  $I_c \simeq 200 \mu\text{A}$ . That is, even if we assume a very small  $J_c$ , we obtain  $I_c \gg I_{\omega_{r,1}}$  and can use the approximation  $\cos \varphi \simeq 1$ . Assuming an oxide thickness on the order of 1 nm, we obtain  $E_{\text{Nb}/\text{Al}}^{\text{rms}} \simeq 0.6 \text{ V m}^{-1}$  from Eq. (4). On the one hand, this field is large enough to mediate a coupling between the TLSs and the resonator. On the other hand, it is small compared to the experimentally observed saturation field  $|\mathbf{E}_{\text{Nb}/\text{Al}}^c| = \sqrt{P_c Z_0}/h_{\text{ox}} \simeq 85 \text{ V m}^{-1}$  derived from the power  $P_c \simeq -124 \text{ dBm}$ .

In the next step, we confirm our model of TLS losses in the interfaces by analyzing the second harmonic mode of sample VIII, which has a voltage antinode at the interface position. As shown in Fig. 7, this mode shows significantly less internal losses than the first harmonic mode. This observation clearly contradicts the expectation  $\delta_i \propto n$  based on a model considering only a uniformly distributed residual conductivity.<sup>43</sup> However, we measure  $\delta_{\text{TLS}}^0 = 7 \times 10^{-6}$  and  $\delta_c = 1.7 \times 10^{-5}$ , that is, values comparable to those of the pure Nb resonator (sample I). Since for the second harmonic mode the interfaces are placed at the current node,  $I_{\omega_{r,2}} \simeq 0$ , the corresponding electric field  $E_{\text{Nb}/\text{Al}}^{\text{rms}}$  is vanishingly small. Therefore, only the TLSs outside the interface, which couple to the resonator electric field, introduce losses comparable to those of sample I (pure Nb). We note that also the power independent contribution  $\delta_c$  is higher for the second harmonic mode than for the first harmonic mode. This behavior

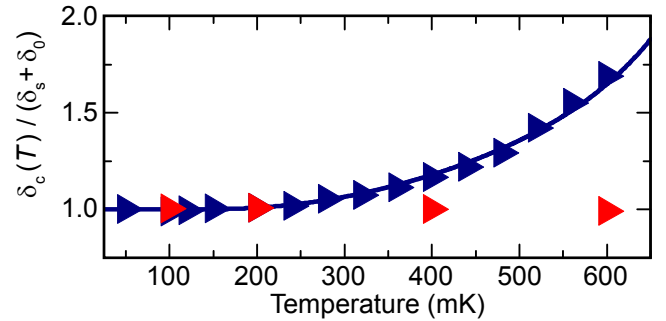


FIG. 8. Normalized losses  $\delta_c(T)/(δ_s + δ_0)$  of sample VIII plotted versus sample temperature. Blue triangles correspond to the first and red triangles to the second harmonic mode. The solid line is a fit of  $\delta_c(T)$  using Eq. (5) based on calculations of  $\delta_{\text{qp}}(T)$ .

indicates that the interfaces are not only strong sources for TLS losses but also for local resistive losses.

Finally, we show that the local losses induced by the interfaces can be significantly reduced by in-situ ion gun treatment of the Nb surface before Al evaporation. Consequently,  $\delta_{\text{TLS}}^0 \simeq 9 \times 10^{-6}$  of the fundamental mode of sample VII (ion gun treatment) is one order of magnitude larger than for sample VIII (no ion gun treatment). As expected, we find that  $\delta_{\text{TLS}}^0$  of sample VII is similar to  $\delta_{\text{TLS}}^0$  of both the second harmonic mode of sample VIII and the fundamental mode of sample I (pure Nb).

### C. Temperature dependent losses in Nb/Al interfaces

We first analyze the temperature dependence of  $P_c$  for both samples including a Nb/Al interface (sample VII and sample VIII). As shown in Fig. 5, the exponent  $\alpha$  is in the same range as for all other samples (see Sec. IV A). Specifically, we extract  $\alpha \simeq 2.6$  (sample VII),  $\alpha = 2.4$  (sample VIII, first harmonic), and  $\alpha = 2.7$  (sample VIII, second harmonic). When extracting  $\alpha$  for the first harmonic of sample VIII, we only take datapoints below 440 mK into account. We attribute the increased slope of  $P_c(T)$  above this temperature to self heating processes<sup>44-47</sup> inside the interfaces. This effect is not present in the second harmonic of sample VIII which has a current node at the interface position.

Next, we study the influence of the Nb/Al interfaces on  $\delta_c$ , i.e., in the high power regime. For pure Nb resonators, we observe no significant change of  $\delta_c$  in the temperature range between 50 mK and 600 mK. This behavior is expected because the number of quasiparticles is negligible for our experiments due to the critical temperature  $T_c \simeq 9 \text{ K}$  of the Nb films. However, the situation is different for samples including an Al strip, which has a lower  $T_c \simeq 1.5 \text{ K}$ . In Fig. 8, we show the temperature dependence of  $\delta_c$  for the first two modes of sample VIII. For the first harmonic mode, we observe a quasiparticle induced increase of  $\delta_c$ , which becomes relevant for temper-

atures above 200 mK. Using  $\delta_s + \delta_0 = 3.6 \times 10^4$  obtained from a power sweep at 50 mK, where quasiparticles are negligible, we fit Eq. (5) to the data and find a kinetic inductance fraction of  $\gamma \simeq 3.5 \times 10^{-4}$ . This value is two orders of magnitude smaller than values reported in literature.<sup>13</sup> We explain this difference by the fact that the length of the Al strip is only 1/100 of the total length of the center conductor. In contrast to the first harmonic mode,  $\delta_c$  of the second harmonic mode shows no temperature dependence because the current distribution of the resonator has a node at the Al position in this case. Hence, the quasiparticles in the Al do not carry a significant amount of the current circulating inside the resonator. Therefore, we conclude that also with respect to quasiparticle losses it is advantageous to place such interfaces at current nodes.

#### D. Eddy current losses

In this subsection we analyze losses resulting from eddy currents which are induced in the conductive material on the backside of the substrate. For this analysis, we compare all CPW samples fabricated by optical lithography. We observe that  $\delta_c$  shows a significant dependence on the substrate thickness as displayed in Fig. 9. Assuming a negligible quasiparticle contribution  $\delta_{qp}(50 \text{ mK}) \simeq 0$ , a numerical fit based on Eq. (5) and Eq. (8) yields  $\delta_0 \simeq 8 \times 10^{-6}$  and  $\sigma_{\omega_r} \simeq 7 \times 10^7 \text{ S m}^{-1}$ . This conductivity is approximately hundred times larger than the room temperature conductivity of silver glue<sup>38</sup> and comparable to the room temperature conductivity of copper.<sup>39,48</sup> Since our experiments are carried out at low temperatures, where the conductivity of metals typically increases by a factor of 100,<sup>49,50</sup> we attribute the observed behavior to ohmic losses in the silver glue used to fix our sample chips. The influence of eddy current losses depends on the material present underneath the sample. Compared to pure metals, silver glue has a relatively low conductivity and therefore larger losses. For samples with a substrate thickness of 525  $\mu\text{m}$  high power losses are already enhanced by 13% compared to  $\delta_0$ . Samples fabricated on 200  $\mu\text{m}$  thick substrates show a loss increase by a factor of four compared to  $\delta_0$ . The slight scatter in  $\delta_c$  for  $h = 250 \mu\text{m}$  is attributed to our assumption of a universal  $\delta_0$ . This assumption is, of course, only a rough estimation because the samples are fabricated with different cleaning methods. In contrast to other groups,<sup>51</sup> we observe an increase of the power independent losses  $\delta_c$  by a factor of three for the sample fabricated with EBL (sample III) compared to sample II, which is fabricated with OL. There are two likely reasons for this observation. First, the Nb edges are smoother for the EBL sample than for the OL samples, resulting in a reduced field elevation at these positions. Second, compared to our OL process, the PMMA resist used for EBL may leave less resist residuals on the sample. Such resist residuals are known to introduce losses.<sup>51</sup>

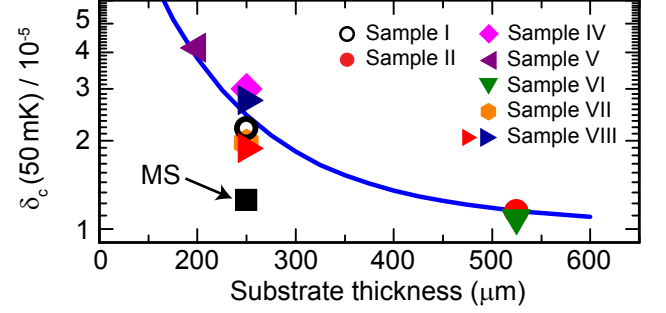


FIG. 9. Power independent losses  $\delta_c$  measured at 50 mK plotted as a function of the substrate thickness. The solid line is a fit based on Eq. (5) and Eq. (8) not accounting for sample IX (MS).

In summary, we can quantitatively explain losses due to eddy currents using numerical calculations of the  $\mathbf{H}$ -field distribution in conductor backed CPW structures. The electrodynamical model suggests that it is advantageous to either use thick substrates or materials with high conductivity on the backside of the substrate. Therefore, losses caused by eddy currents can be avoided by using superconducting materials at this position. This conclusion is supported by our measurements on the MS resonator (sample IX), which is fabricated on a 250  $\mu\text{m}$  thick substrate and employs a superconducting ground plane. For this sample, we measure  $\delta_c \simeq 1 \times 10^{-5}$ , which is reduced compared to the values of the other samples fabricated on a 250  $\mu\text{m}$  thick substrate by a factor of two, despite the fact that the field at the bottom surface of the substrate is an order of magnitude larger compared to the CPW samples.

## V. CONCLUSIONS

We fabricate superconducting CPW resonators and analyze mechanisms leading to microwave losses. With respect to TLS losses, we find that the characteristic power necessary to saturate TLSs shows a pronounced temperature dependence. Specifically, we extract an exponent  $\alpha = 2.5$  for the polynomial part of this temperature dependence. Furthermore, we show that an HF-dip can be used to remove TLSs and therefore reduce losses on oxide covered silicon substrates. In addition, we investigate resonators containing Nb/Al interfaces, which typically occur for galvanically coupled quantum circuits. We quantitatively investigate the temperature and power dependence of the losses caused by these interfaces. These losses can be reduced by either placing the interfaces in a current node or by removing the oxide layer containing the TLSs by in-situ Ar ion milling. In the high power limit, where the TLSs are saturated, we observe temperature dependent losses induced by quasiparticle excitations in the Al. Finally, we investigate losses generated by eddy currents in the conductive

material on the backside of the substrate. Our results show that the usage of thick enough substrates or metals with high conductivity on the substrate backside helps to minimize these losses.

This work is supported by the German Research Foundation through SFB 631 and FE 1564/1-1, EU projects CCQED, PROMISCE, the doctorate program ExQM of the Elite Network of Bavaria.

- <sup>1</sup>R. J. Schoelkopf and S. M. Girvin, *Nature* **451**, 664 (2008).
- <sup>2</sup>T. Niemczyk, F. Deppe, H. Hübl, E. P. Menzel, F. Hocke, M. J. Schwarz, J. J. Garcia-Ripoll, D. Zueco, T. Hümmer, E. Solano, A. Marx, and R. Gross, *Nat. Phys.* **6**, 772 (2010).
- <sup>3</sup>Y. Kubo, C. Grezes, A. Dewes, T. Umeda, J. Isoya, H. Sumiya, N. Morishita, H. Abe, S. Onoda, T. Ohshima, V. Jacques, A. Dreau, J.-F. Roch, I. Diniz, A. Auffeves, D. Vion, D. Esteve, and P. Bertet, *Phys. Rev. Lett.* **107**, 220501 (2011).
- <sup>4</sup>M. Mariantoni, H. Wang, R. C. Bialczak, M. Lenander, E. Lucero, M. Neeley, A. D. O'Connell, D. Sank, M. Weides, J. Wenner, T. Yamamoto, Y. Yin, J. Zhao, J. M. Martinis, and A. N. Cleland, *Nat. Phys.* **7**, 287 (2011).
- <sup>5</sup>M. Hofheinz, H. Wang, M. Ansmann, R. C. Bialczak, E. Lucero, M. Neeley, A. D. O'Connell, D. Sank, J. Wenner, J. M. Martinis, and A. N. Cleland, *Nature* **459**, 546 (2009).
- <sup>6</sup>D. S. Wisbey, J. Gao, M. R. Vissers, F. C. S. da Silva, J. S. Kline, L. Vale, and D. P. Pappas, *J. Appl. Phys.* **108**, 093918 (2010).
- <sup>7</sup>J. Wenner, R. Barends, R. C. Bialczak, Y. Chen, J. Kelly, E. Lucero, M. Mariantoni, A. Megrant, P. J. J. O'Malley, D. Sank, A. Vainsencher, H. Wang, T. C. White, Y. Yin, J. Zhao, A. N. Cleland, and J. M. Martinis, *Appl. Phys. Lett.* **99**, 113513 (2011).
- <sup>8</sup>J. M. Sage, V. Bolkhovsky, W. D. Oliver, B. Turek, and P. B. Welander, *J. Appl. Phys.* **109**, 063915 (2011).
- <sup>9</sup>S. Ohya, B. Chiaro, A. Megrant, C. Neill, R. Barends, Y. Chen, J. Kelly, D. Low, J. Mutus, P. J. J. O'Malley, P. Roushan, D. Sank, A. Vainsencher, J. Wenner, T. C. White, Y. Yin, B. D. Schultz, C. J. Palmstrom, B. A. Mazin, A. N. Cleland, and J. M. Martinis, *Supercond. Sci. Tech.* **27**, 015009 (2014).
- <sup>10</sup>A. D. O'Connell, M. Ansmann, R. C. Bialczak, M. Hofheinz, N. Katz, E. Lucero, C. McKenney, M. Neeley, H. Wang, E. M. Weig, A. N. Cleland, and J. M. Martinis, *Appl. Phys. Lett.* **92**, 112903 (2008).
- <sup>11</sup>M. Arzeo, F. Lombardi, and T. Bauch, *Appl. Phys. Lett.* **104**, 212601 (2014).
- <sup>12</sup>R. Barends, J. Wenner, M. Lenander, Y. Chen, R. C. Bialczak, J. Kelly, E. Lucero, P. O' Malley, M. Mariantoni, D. Sank, H. Wang, T. C. White, Y. Yin, J. Zhao, A. N. Cleland, J. M. Martinis, and J. J. A. Baselmans, *Appl. Phys. Lett.* **99**, 113507 (2011).
- <sup>13</sup>J. Gao, J. Zmuidzinas, A. Vayonakis, P. Day, B. Mazin, and H. Leduc, *J. Low Temp. Phys.* **151**, 557 (2008).
- <sup>14</sup>T. Lindström, J. E. Healey, M. S. Colclough, C. M. Muirhead, and A. Y. Tzalenchuk, *Phys. Rev. B* **80**, 132501 (2009).
- <sup>15</sup>M. S. Khalil, M. J. A. Stoutimore, F. C. Wellstood, and K. D. Osborn, *J. Appl. Phys.* **111**, 054510 (2012).
- <sup>16</sup>U. Fano, *Phys. Rev. Lett.* **124**, 1866 (1961).
- <sup>17</sup>A. Megrant, C. Neill, R. Barends, B. Chiaro, Y. Chen, L. Feigl, J. Kelly, E. Lucero, M. Mariantoni, P. O'Malley, D. Sank, A. Vainsencher, J. Wenner, T. White, Y. Yin, J. Zhao, C. Palmstrom, J. M. Martinis, and A. Cleland, *Appl. Phys. Lett.* **100**, 113510 (2012).
- <sup>18</sup>J. Wenner, M. Neeley, R. C. Bialczak, M. Lenander, E. Lucero, A. D. O'Connell, D. Sank, H. Wang, M. Weides, A. N. Cleland, and J. M. Martinis, *Supercond. Sci. Tech.* **24**, 065001 (2011).
- <sup>19</sup>J. M. Hornbrook, E. E. Mitchell, and D. J. Reilly, (2012), arXiv:1203.4442 [cond-mat].
- <sup>20</sup>M. Watanabe, K. Inomata, T. Yamamoto, and J.-S. Tsai, *Phys. Rev. B* **80**, 174502 (2009).
- <sup>21</sup>A. J. Leggett, S. Chakravarty, A. T. Dorsey, M. P. A. Fisher, A. Garg, and W. Zwerger, *Rev. Mod. Phys.* **59**, 1 (1987).
- <sup>22</sup>W. A. Phillips, *Rep. Progr. Phys.* **50**, 1657 (1987).
- <sup>23</sup>T. Niemczyk, F. Deppe, M. Mariantoni, E. P. Menzel, E. Hoffmann, G. Wild, L. Eggenstein, A. Marx, and R. Gross, *Supercond. Sci. Tech.* **22**, 034009 (2009).
- <sup>24</sup>U. Strom, M. von Schickfus, and S. Hunklinger, *Phys. Rev. Lett.* **41**, 910 (1978).
- <sup>25</sup>H. Wang, M. Hofheinz, J. Wenner, M. Ansmann, R. C. Bialczak, M. Lenander, E. Lucero, M. Neeley, A. D. O'Connell, D. Sank, M. Weides, A. N. Cleland, and J. M. Martinis, *Appl. Phys. Lett.* **95**, 233508 (2009).
- <sup>26</sup>M. V. Schickfus and S. Hunklinger, *Phys. Lett. A* **64**, 144 (1977).
- <sup>27</sup>J. Jäckle, *Z. Phys.* **257**, 212 (1972).
- <sup>28</sup>S. Rudin, T. L. Reinecke, and B. Segall, *Phys. Rev. B* **42**, 11218 (1990).
- <sup>29</sup>P. Borri, W. Langbein, J. M. Hvam, and F. Martelli, *Phys. Rev. B* **59**, 2215 (1999).
- <sup>30</sup>J. Lisenfeld, A. Lukashenko, M. Ansmann, J. M. Martinis, and A. V. Ustinov, *Phys. Rev. Lett.* **99**, 170504 (2007).
- <sup>31</sup>J. Lisenfeld, C. Müller, J. H. Cole, P. Bushev, A. Lukashenko, A. Shnirman, and A. V. Ustinov, *Phys. Rev. Lett.* **105**, 230504 (2010).
- <sup>32</sup>J. M. Martinis, K. B. Cooper, R. McDermott, M. Steffen, M. Ansmann, K. D. Osborn, K. Cicak, S. Oh, D. P. Pappas, R. W. Simmonds, and C. C. Yu, *Phys. Rev. Lett.* **95**, 210503 (2005).
- <sup>33</sup>D. Kasilingam and D. Rutledge, in *Microwave Symposium Digest, IEEE MTT-S International* (1983) pp. 113–116.
- <sup>34</sup>T. Noguchi, M. Naruse, and Y. Sekimoto, *Phys. Procedia* **36**, 318 (2012).
- <sup>35</sup>D. C. Mattis and J. Bardeen, *Phys. Rev.* **111**, 412 (1958).
- <sup>36</sup>S. P. Morgan, *J. Appl. Phys.* **20**, 352 (1949).
- <sup>37</sup>R. Simons and R. Arora, *IEEE T. Microw. Theory* **30**, 1094 (1982).
- <sup>38</sup>“Product no. 16062 - pelco conductive silver paint,” Tech. Rep. (TED PELLA. INC., 2013).
- <sup>39</sup>E. Maxwell, *J. Appl. Phys.* **18**, 629 (1947).
- <sup>40</sup>A. V. Shcherbakova, K. G. Fedorov, K. V. Shulga, V. V. Ryazanov, V. V. Bolginov, V. A. Oboznov, S. V. Egorov, V. O. Shkolnikov, M. J. Wolf, D. Beckmann, and A. V. Ustinov, *Supercond. Sci. Tech.* **28**, 025009 (2015).
- <sup>41</sup>V. E. Manucharyan, E. Boaknin, M. Metcalfe, R. Vijay, I. Siddiqi, and M. Devoret, *Phys. Rev. B* **76**, 014524 (2007).
- <sup>42</sup>A. Kleinsasser, R. Miller, and W. Mallison, *IEEE T. Appl. Supercon.* **5**, 26 (1995).
- <sup>43</sup>M. Göppl, A. Fragner, M. Baur, R. Bianchetti, S. Filipp, J. M. Fink, P. J. Leek, G. Puebla, L. Steffen, and A. Wallraff, *J. Appl. Phys.* **104**, 113904 (2008).
- <sup>44</sup>K. Lang, S. Nam, J. Aumentado, C. Urbina, and J. M. Martinis, *IEEE T. Appl. Supercon.* **13**, 989 (2003).
- <sup>45</sup>E. A. Tholen, A. Ergül, E. M. Doherty, F. M. Weber, F. Gregis, and D. B. Haviland, *Appl. Phys. Lett.* **90**, 253509 (2007).
- <sup>46</sup>H. B. Wang, T. Hatano, T. Yamashita, P. H. Wu, and P. Müller, *Appl. Phys. Lett.* **86**, 023504 (2005).
- <sup>47</sup>S. Guénon, M. Grünzweig, B. Gross, J. Yuan, Z. G. Jiang, Y. Y. Zhong, M. Y. Li, A. Iishi, P. H. Wu, T. Hatano, R. G. Mints, E. Goldobin, D. Koelle, H. B. Wang, and R. Kleiner, *Phys. Rev. B* **82**, 214506 (2010).
- <sup>48</sup>J. Thorp, *Proc. of the IEEE - Part III: Radio and Communication Engineering* **101**, 357 (1954).
- <sup>49</sup>R. A. Matula, *J. Phys. Chem. Ref. Data* **8**, 1147 (1979).
- <sup>50</sup>M. Fouaidy and N. Hammoudi, *Physica C* **441**, 137 (2006).
- <sup>51</sup>C. M. Quintana, A. Megrant, Z. Chen, A. Dunsworth, B. Chiaro, R. Barends, B. Campbell, Y. Chen, I.-C. Hoi, E. Jeffrey, J. Kelly, J. Y. Mutus, P. J. J. O'Malley, C. Neill, P. Roushan, D. Sank, A. Vainsencher, J. Wenner, T. C. White, A. N. Cleland, and J. M. Martinis, *Appl. Phys. Lett.* **105**, 062601 (2014).